Iraqi Journal of Science, 2024, Vol. 65, No. 8, pp: 4313-4324
DOI: 10.24996/ijs.2024.65.8.16

ISSN: 0067-2904

Studying the Gas Sensitivity and Magnetic Properties of Magnesium Ferrite Prepared by the Sol-Gel Route

Hussein I. Mahdi [1], Nabeel A. Bakr [1], Tagreed M. Al-Saadi [2]
[1]*Department of Physics, College of Science, University of Diyala, Diyala, IRAQ*
[2] *College of Education for Pure Science, Ibn Al Haitham, University of Baghdad, Baghdad, IRAQ*

Received: 18/5/2023 Accepted: 19/10/2023 Published: 30/8/2024

Abstract

Nickel-doped manganese–magnesium ferrite ($Ni_xMn_{0.25-x}Mg_{0.75}Fe_2O_4$) was prepared using the auto-combustion method. X-ray diffraction patterns showed a single ferrite spinel phase in all the prepared samples. The crystallite size ranged from 24.30 to 28.32 nm, increasing with increasing the Ni content. The porous structure of all the samples was verified with a scanning electron microscope. FE-SEM images were used to confirm the production of spherical or semi-spherical nanoparticles with little change in particle size distribution. The study revealed that the nanoparticles were small enough to behave superparamagnetically. According to the magnetic tests conducted with the VSM at room temperature, the hysteresis loop region is practically non-existent, indicating typical soft magnetic materials. In addition, the conductance responses of the magnesium ferrite nanocomposite were measured by exposing it to the oxidizing gas (NO_2) at different operating temperatures. The results showed that the sensor with the nano ferrite sample of (x = 0.20) has a good sensitivity of 707.22% as well as response and recovery times.

Keywords: Magnesium ferrite, Nitrogen dioxide gas, Sensitivity, Response time, Recovery time.

دراسة تحسسية الغاز والخصائص المغناطيسية لفرايت المغنسيوم المحضر بطريقة السول–جل

حسين مهدي[1] ، نبيل بكر[1] ، تغريد مسلم[2]
[1] كلية العلوم ، جامعة ديالى, العراق
[2] كلية التربية ابن الهيثم ، جامعة بغداد, العراق

الخلاصة

في هذا البحث تم تحضير فرايت المغنيسيوم–المنغنيز المشوب بالنيكل باستخدام طريقة الاحتراق الذاتي. أظهرت أنماط حيود الأشعة السينية طور واحد من الفريت نوع سبينل لجميع العينات المنتجة. تراوح حجم البلورات من 24.30 إلى 28.32 نانومتر مع زيادة محتوى النيكل. تم الحصول على البنية المسامية لجميع العينات المدروسة تحت المجهر الإلكتروني الماسح. تم استخدام صور FE–SEM لتأكيد إنتاج الجسيمات النانوية الكروية أو شبه الكروية مع تغيير طفيف في توزيع حجم الجسيمات. كشفت الدراسة أن الجسيمات النانوية كانت صغيرة بما يكفي لتتصرف في مجال مغناطيسي فائق. وفقًا للاختبارات المغناطيسية التي تم

*Email: taghreed.m.m@ihcoedu.uobaghdad.edu.

إجراؤها باستخدام VSM في درجة حرارة الغرفة، فإن منطقة حلقة التباطؤ غير موجودة عمليًا، مما يشير إلى وجود مواد مغناطيسية ناعمة نموذجية. أيضًا، من خلال تعريض مركب فرايت المغنيسيوم النانوي لغاز مؤكسد (NO_2)في درجات حرارة تشغيل مختلفة، تم قياس استجابات للفرايت لغاز NO_2. وأظهرت النتائج أن المستشعر يتمتع بحساسية أفضل، حيث بلغت 707.22٪ للعينة عند (x = 0.20) للفرايت النانوي، وكانت أوقات الاستجابة والاسترداد صغيرة.

1. Introduction

Because chemical sensors may control emissions and identify dangerous contaminants, their demand has risen dramatically. The most promising chemical sensors are metal oxide semiconductor since they offer several benefits like low cost, compact size, low power consumption, and online operation. They have received extensive research for a long time because they are very suitable for microelectronic processes [1]. Utilizing nanocrystalline materials for gas sensing has recently sparked a great deal of curiosity [2]. Ferrites have proven to be effective materials for gas semiconductor detectors [3]. The conductivity of the detecting material of a semiconductor gas sensor is modified when it is exposed to various gas environments.

The surface-controlled technique of gas sensing depends on the interaction among both gas molecules to be identified and adsorbed oxygen. The operating temperature, the type of gas being used, and the type of detector all affect how the detector responds to gas [4]. The oxides with a structural formula of AB_2O_4 are significant for gas detection purposes and were studied for identifying oxidizing and reducing gases. These oxides are preferred above all spinel-type metal oxide semiconductor detectors due to the employment of magnetic materials in high-frequency applications for microelectronic/magnetic devices [5]. The most exciting features of spinel ferrites for gas detection are their chemical makeup and structure, in which transition or post-transition cations occupy two different cation positions [6]. The spinel ferrites, including $MgFe_2O_4$, $CoFe_2O_4$, $ZnFe_2O_4$, $NiFe_2O_4$, and $MnFe_2O_4$, have shown excellent sensitivity for a wide range of gases due to their stability in thermal and chemical atmospheres, quick reaction and recovery times, inexpensive, and straightforward electronic structures [7, 8]. Magnesium ferrite is one of the most significant ferrites due to its low magnetic and dielectric losses, high resistivity, and other characteristics that make it a vital part of catalytic reactions, detectors, and adsorption [9]. It has an inverse spinel structure with Mg^{2+} ions at octahedral sites and Fe^{3+} ions evenly distributed over tetrahedral and octahedral sites, dependent on the divalent and trivalent ions' preferred energies in the spinel structure [10].

The sol-gel, molten-salt approach, hydrothermal, co-precipitation, and microemulsion techniques were all employed to obtain nano-sized spinel ferrite powder [11,12]. Among these various techniques, the sol-gel technique is a convenient, environmentally friendly, and low-cost technique for synthesizing ferrites at relatively low temperatures in a short period [13].

Doping is an effective and successful method for fine-tuning the required properties of semiconductors [14]. The dopant might improve the gas-sensing characteristics of metal-oxide semiconductors by modifying the energy-band structure, improving the morphology and surface-to-volume ratio, and developing extra active centers at the grain boundaries [15].

In the present work, the synthesis of $Ni_xMn_{0.25-x}Mg_{0.75}Fe_2O_4$ nano-ferrite is reported using the simple sol-gel auto-combustion technique. Its application as NO_2 gas sensor has been systematically investigated, and the results are presented and discussed.

2. Experimental Part

2.1. Materials and method

Spinel ferrite of the general formula ($Ni_xMn_{0.25-x}Mg_{0.75}Fe_2O_4$) was synthesized (where x= 0.05, 0.10, 0.15, 0.20) using the sol-gel auto-combustion method. Analytical-grade materials of ferric nitrate nonahydrate $Fe(NO_3)_3.9H_2O$, magnesium nitrate hexahydrate $Mg(NO_3)_2.6H_2O$, manganese nitrate monohydrate $Mn(NO_3)_2.H_2O$, and nickel nitrate hexahydrate $Ni(NO_3)_2.6H_2O$ were used as precursors of iron and other metals, whereas citric acid ($C_6H_8O_7$) was used as a complexant/fuel agent for the auto-combustion process. The required masses of the raw materials required to prepare the ferrite are shown in Table 1. These values were obtained using the following equation [16]:

$$\mathrm{Wt\ (g)} = \mathrm{M_w\ (g/mol)} \times \mathrm{M\ (mol/L)} \times \mathrm{V\ (L)} \qquad \ldots\ldots\ldots\ldots\ldots\ldots (1)$$

Where: Wt is the mass of the raw material, M_w is the molecular weight of the raw material, M is the number of moles required of the material in one liter of solvent, and V is the volume of solvent.

Metal nitrates were entirely dissolved in small quantities of distilled water after being weighed. This solution was mixed with citric acid to achieve a molar ratio 1:1 nitrates: citric acid in the final sample. After that, ammonia was added to the mixture dropwise while mixing to balance the (pH) to (~7). A combustion reaction occurs among the metal nitrates and citrate molecules, producing in a polymer network with colloidal dimensions recognized as sol [17-19]. While continuously mixing and heating the solution for one hour at 90 °C, the solution was evaporated. Then it was held at this temperature until it was solidified into a gel form. The gel was then cooked to 120 ◦C to trigger auto-combustion, and the dried gel was burnt until it was consumed to produce a loose powder. Finally, the resultant powder was crushed in an agate mortar to get the required ferrite. The freshly as-prepared ferrite powder was then heated for two hours at 600 ◦C.

Table 1: The masses of raw materials required to obtain $Ni_xMn_{0.25-x}Mg_{0.75}Fe_2O_4$ ferrite.

x	Composition	Ferric nitrate (g)	Magnesium nitrate (g)	Manganese nitrate (g)	Nickel nitrate (g)	Citric acid (g)
0.00	$Mn_{0.25}Mg_{0.75}Fe_2O_4$	32.32	7.6923	1.8900	0.00	23.0556
0.05	$Ni_{0.05}Mn_{0.20}Mg_{0.75}Fe_2O_4$	32.32	7.6923	1.5120	0.5816	23.0556
0.10	$Ni_{0.10}Mn_{0.15}Mg_{0.75}Fe_2O_4$	32.32	7.6923	1.1340	1.1632	23.0556
0.15	$Ni_{0.15}Mn_{0.10}Mg_{0.75}Fe_2O_4$	32.32	7.6923	0.7560	1.7448	23.0556
0.20	$Ni_{0.20}Mn_{0.05}Mg_{0.75}Fe_2O_4$	32.32	7.6923	0.3780	2.3264	23.0556

2.2. Fabrication of gas sensors

For each sample, 1.75 g of the prepared ferrite powder was subjected to a pressure of 200 bar by a manual press for 120 seconds to produce a disc with a diameter of 1 cm and a thickness of 3.5 mm. The disc was then placed in a furnace at a temperature of 900 ◦C for two hours. Thin copper wires were used as connecting leads, and silver paste was used to construct the electrodes on one side of the sample; electrodes were placed on all sample surfaces to obtain Ohmic contacts [20]. The electrodes were fabricated for the five nano-ferrite samples. The sensitivity of each sample to NO_2 gas at a constant concentration (65 ppm) was tested by a gas sensitivity test system.

Gas concentration, material composition, type of conductivity, operating temperature, and different controlling parameters are considered important factors which affect the gas sensitivity or gas response of the metal oxide semiconductor sensor [21]. Depending on the compound and operating temperature, the gas sensitivity of the nano-ferrite to NO_2 gas was studied and computed using the following equation:

$$S = \left| \frac{Rg - Ra}{Ra} \right| \times 100\ \% \qquad \text{[Oxidizing gas]} \qquad \ldots\ldots\ldots\ldots\ldots (2)$$

Where: R_g and R_a represent the electrical resistances in the NO_2 gas and air, respectively [22,23].

The response time is defined as the amount of time needed to reach 90% of the equilibrium response of the gas, while the recovery time, is defined as the amount of time needed to reach 10% of the baseline resistance [24].

2.3. Characterization

With a powder X-ray diffractometer (Philips PW1730), the ferrites' X-ray diffraction (XRD) patterns were obtained via Cu-Kα of 1.5406 Å wavelength radiation, scan range: 20^o – 80^o, and scan speed: 6 deg./min. The ferrites' surface morphology was investigated utilizing (MTRA3 LMU) Field Emission Scanning Electron Microscope (FE-SEM) combined with Energy Dispersive X-ray Analyzer (EDX). A vibrating sample magnetometer (EZ VSM model 10) was used to measure the magnetism of some specimens. To detect (NO_2) gas at various temperatures, the gas response characteristics of sintered discs (900°C) were investigated. The resistance of gas sensor samples was measured with an Impedance Analyzer (UNI-TUT81B) equipped with a computerized testing tool.

3. Results and Discussion

3.1. X-Ray Diffraction

X-ray diffraction (XDR) analysis was carried out to determine the phase formation of the magnesium-ferrite in the 2θ range $10^o \leq 2\theta \leq 80^o$. Figure 1 shows the indexed X-ray diffraction patterns of the $Ni_xMn_{0.25-x}Mg_{0.75}Fe_2O_4$ ferrite annealed at 600 ◦C. The presence of (220), (311), (400), (422), (511), (440), and (533) planes confirms the formation of cubic spinel structure. The diffraction peaks agree with the JCPDS card number 89-3084 [25]. Additionally, the size of the crystallites gradually decreased as the amount of Ni doping increased. This was shown in the XRD patterns, where the $Ni_xMn_{0.25-x}Mg_{0.75}Fe_2O_4$ nano-peaks were shifted to higher angle values, as listed in Table 2.

Using Scherrer's equation, the crystallite sizes D of the $Ni_xMn_{0.25-x}Mg_{0.75}Fe_2O_4$ samples were determined from the broadening of the (311) peak in the XRD patterns.

$$D = \frac{K\lambda}{\beta \cos\theta} \qquad \ldots\ldots\ldots\ldots\ldots (3)$$

Where: K is a constant assumed to be 0.9, λ is the X-ray wavelength equal to 1.5406 (Å), β is the Full Width at Half Maximum (FWHM) of the highest intensity diffraction peak expressed in radians, while θ is the Bragg's angle of the diffraction peak [26,27].

Using the following equation, the cubic unit cell lattice parameter (a) for all compounds was computed via diffraction planes:

$$a = d_{hkl}\sqrt{h^2 + k^2 + I^2} \qquad \ldots\ldots\ldots\ldots\ldots (4)$$

Where: d is the interplanar spacing and (h, k, l) are the Miller indices of the crystal planes [28]. The following equation was used to compute the theoretical density (ρ_x):

$$\rho_x = \frac{8\,M_W}{N_A\,a^3} \qquad \ldots\ldots\ldots\ldots\ldots (5)$$

Where: M_W represents the molecular weight, and N_A is Avogadro's number [29,30].

The lattice parameter (a), XRD density (ρ_x), and crystallite size (D) for all samples are given in Table 3.

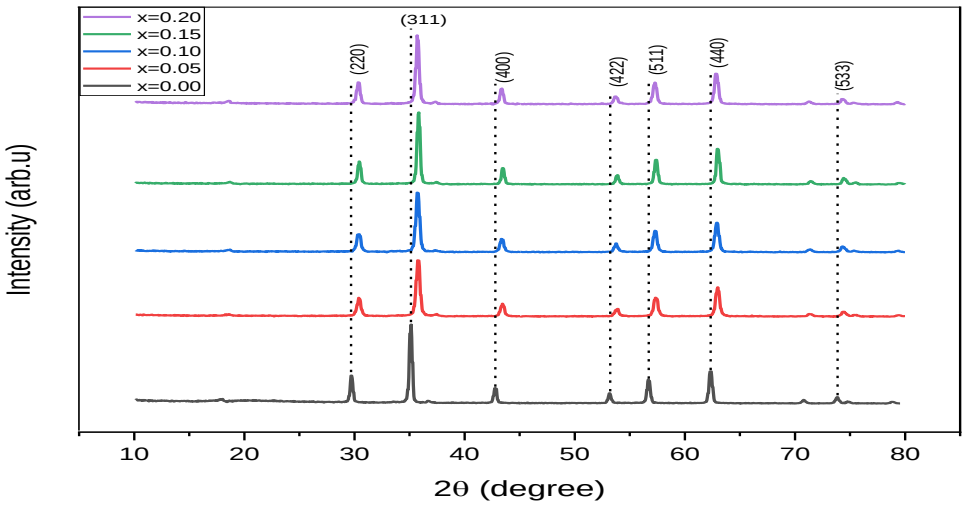

Figure 1: X-ray diffraction patterns of $Ni_xMn_{0.25-x}Mg_{0.75}Fe_2O_4$ nano-ferrite prepared by auto-combustion method.

Increasing the concentration of Ni^{2+} led to an increase in the lattice constant of the ferrite compounds, as listed in Table 3. Smaller Fe^{3+} ions migrate from tetrahedral to octahedral positions in response to Ni^{2+} addition [31,32]. Therefore, tetrahedral sites are enlarged as a result of the lattice constant increase [33,34]. Moreover, this caused the lattice to grow and the density to drop, indicating that the lattice constant has changed as a result of the dopant ions being absorbed into the lattice could have taken an interstitial position among the hosting ions [20].

Table 2: Structure properties of the Magnesium ferrite

h k l	2θ (deg) (JCPDS)	2θ (deg) (x=0.00)	2θ (deg) (x=0.05)	2θ (deg) (x=0.10)	2θ (deg) (x=0.15)	2θ (deg) (x=0.20)
220	30.115	30.1365	30.4563	30.3111	30.3932	30.3938
311	35.466	35.4950	35.8238	35.7308	35.8876	35.7541
400	43.123	43.2299	43.5441	43.4461	43.4725	43.3345
422	53.478	53.5835	53.9189	53.7877	53.8403	53.6563
511	57.000	57.1528	57.4708	57.3573	57.4057	57.2337
440	62.594	62.7239	62.8946	62.9067	62.9564	62.8185
533	74.049	74.2529	74.3735	74.2861	74.3755	74.2936

Table 3: Unit cell constant (a), density (ρx) and crystallite size (D) of NixMn0.25-xMg0.75Fe2O4 nano-ferrite prepared by auto-combustion method.

x	Composition	a (Å)	ρ_x (g/cm^3)	D (nm)
0.00	$Mn_{0.25}Mg_{0.75}Fe_2O_4$	8.36743	5.250	28.31
0.05	$Ni_{0.05}Mn_{0.20}Mg_{0.75}Fe_2O_4$	8.37691	5.232	24.34
0.10	$Ni_{0.10}Mn_{0.15}Mg_{0.75}Fe_2O_4$	8.38131	5.224	24.34
0.15	$Ni_{0.15}Mn_{0.10}Mg_{0.75}Fe_2O_4$	8.38245	5.222	28.32
0.20	$Ni_{0.20}Mn_{0.05}Mg_{0.75}Fe_2O_4$	8.38717	5.213	24.30

3.2. FE-SEM and EDX Analysis

To assess the morphology of the fabricated samples, (FE-SEM) was used. Figure 2 illustrates the $Ni_xMn_{0.25-x}Mg_{0.75}Fe_2O_4$ nano-ferrite micro images at a 200 nm scale after annealing at 600 °C. The observed FE-SEM images made it extremely apparent that the magnetic ferrite particles were created through some aggregation at the nanoscale. The FE-SEM images show porous, sponge-like shape particles for the samples with x = 0.00 and 0.05. Most likely, the gases released during the gel's combustion process caused the pores to form [35]. In addition, the images show spherical or semi-spherical particles and nonhomogeneous in the samples with x=0.10 and 0.15. The images also show homogeneous distribution and spherical nanoparticles of the samples with x = 0.20. The FE-SEM images show the formation of tiny agglomerated grains with surface spaces or voids and no distinct shape. The porosity is found in the agglomerates. The described porous microstructure is advantageous for sensing since gas detection is a surface phenomenon, and porosity is crucial [36]. The micrographs make clear that the nano ferrite's structures are extremely coarse, which makes it easier for oxygen species to bind to the detecting surface. The adsorption of oxygen species is responsible for gas detection [37].

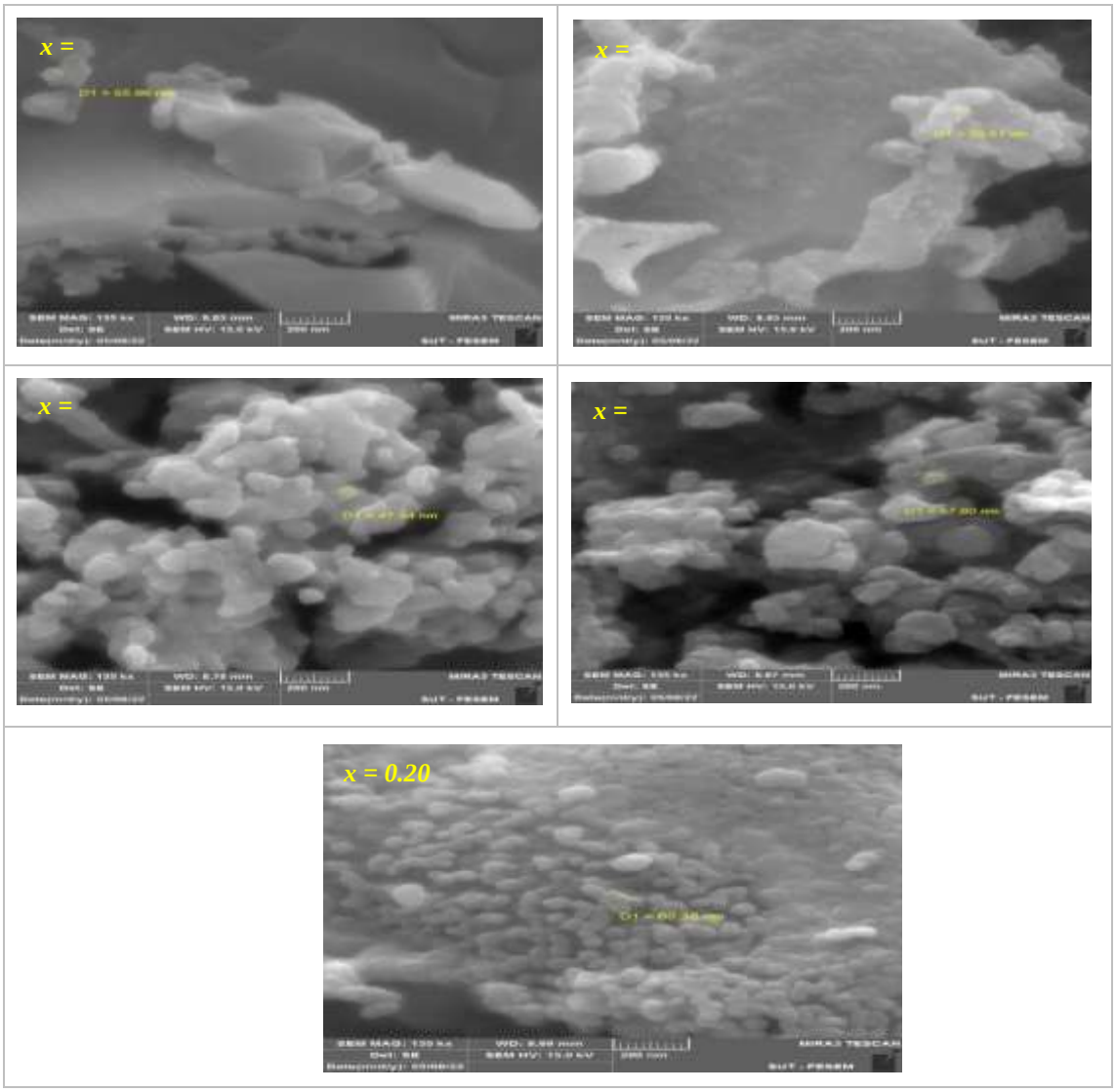

Figure 2: FE-SEM images of $Ni_xMn_{0.25-x}Mg_{0.75}Fe_2O_4$ nano-ferrite.

The EDX spectra of the magnesium-ferrite compound is illustrated in Figure 3. The spectral lines are related to (Ni, Mn, Mg, Fe and O), verifying that the synthesized compound $Ni_xMn_{0.25-x}Mg_{0.75}Fe_2O_4$ was achieved.

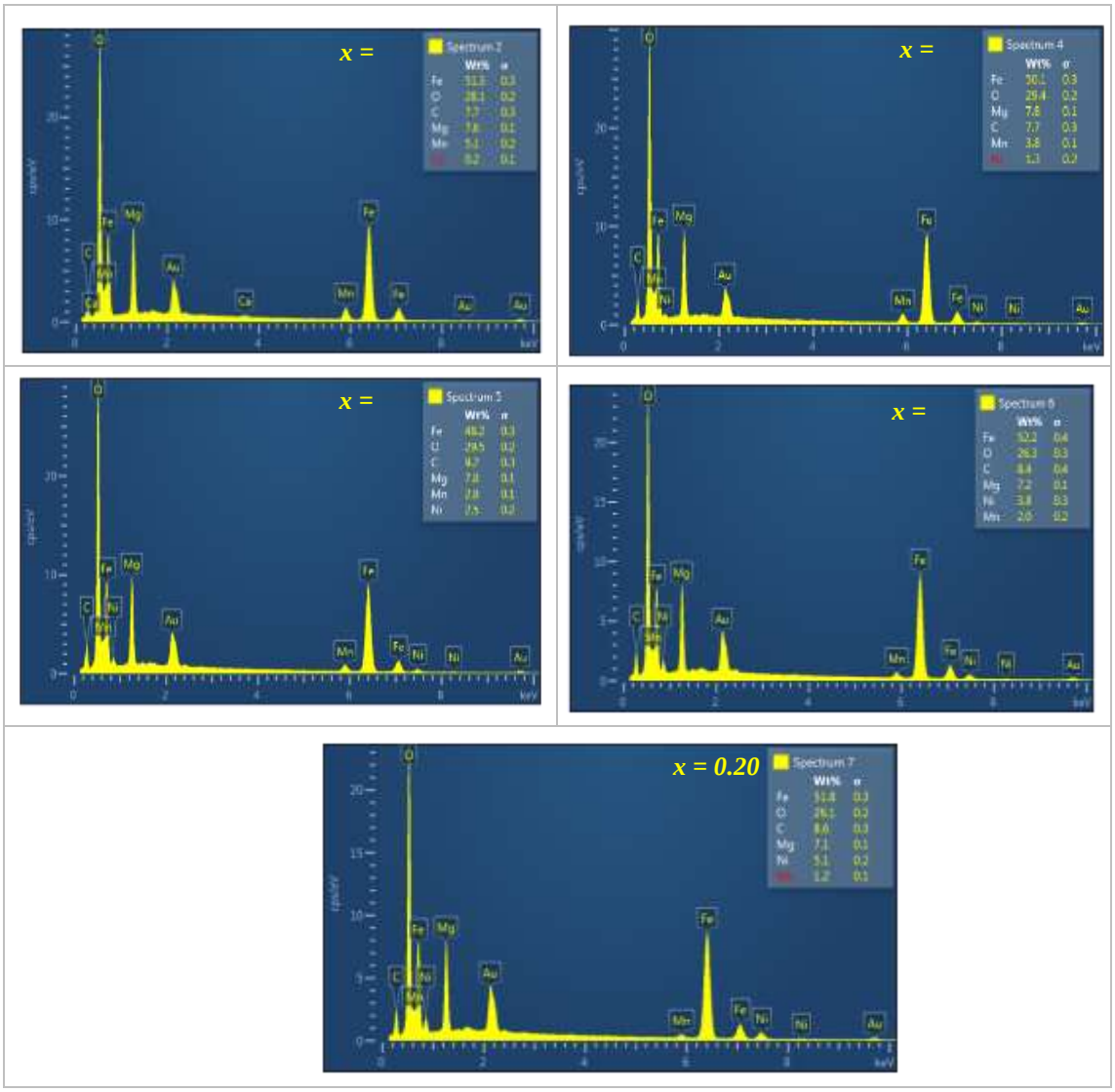

Figure 3: EDX spectra of $Ni_xMn_{0.25-x}Mg_{0.75}Fe_2O_4$ nano-ferrite.

3.4. Magnetic Characteristics

The magnetic characteristics of the samples were examined at room temperature (300 K). The hysteresis loop curves of $Ni_xMn_{0.25-x}Mg_{0.75}Fe_2O_4$ with x = 0.00 and 0.20 were measured with a vibrating sample magnetometer (EZ VSM model 10), as shown in Figure 4. The (S) shaped curves indicate that standard soft magnetic material and magnetic coercivity can be ignored. The particles also exhibit superparamagnetic behavior due to their small size. Small crystallite size was evidenced by the XRD analysis, as shown in Table 3, this causes the nanoparticles to exhibit superparamagnetic behavior, where their magnetic moments attempt to align with one another in a specific way [38,39].

According to Neel theory, the distribution of cations among the octahedral and tetrahedral locations in spinel ferrite determines the overall magnetic moment [29,39]. The saturation magnetization (M_s), remnant magnetization (M_r), and magnetic coercivity (H_c) values were computed from the M-H (Magnetization vs applied magnetic field) curves depending on (M_s) measured values.

M-H curves demonstrate how a chemical compound affects magnetic properties. Table 4 illustrates the variation in saturation magnetization values (M_s) for the $Ni_xMn_{0.25-x}Mg_{0.75}Fe_2O_4$ samples captured from hysteresis loop curves. As 0.20 of the Ni^{2+} ions in the structure were substituted out for Mn^{2+} ions, the M_s value dropped from 28.980 (emu/g) for x = 0.00 to 23.400 (emu/g) for x = 0.20. According to the experimental observations, as nickel content increased, the ratio of ferric, manganese, or magnesium ions on the A-location decreased. At the same time, the Fe^{3+} ions grew by the same amount octahedral B site. As a result, the interactions between the metal ions in the tetrahedral A site and the octahedral B site was reduced. As a consequence of the ionic moments on the octahedral B-sites being no longer maintained parallel to each other, the angles among them start to form, which lowers the moment of the octahedral B-sites sub lattice itself. Most likely, nickel ions were replaced by cations in the octahedral B-sites [39]. Figure 4 shows that the observed values of the remnant magnetization (M_r) and coercive field (H_c) are very small, demonstrating that the grain size does not pass the critical diameter of a single-domain grain [39]. The cation distribution has a significant impact on the net magnetic moments and magnetocrystalline anisotropy. Table 4 lists the magnetic factors.

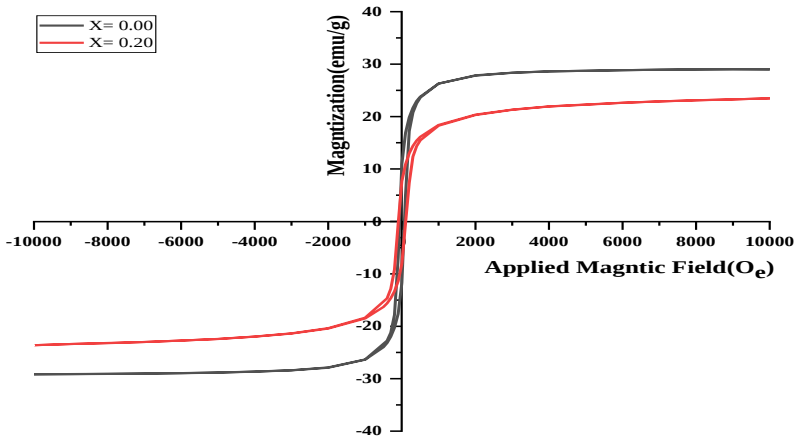

Figure 4: Magnetization (M) versus applied magnetic field (O_e) of $Ni_xMn_{0.25-x}Mg_{0.75}Fe_2O_4$ (x = 0.00, and 0.20) nanoparticles at 300K.

Table 4: Variation of magnetic factors for $Ni_xMn_{0.25-x}Mg_{0.75}Fe_2O_4$ (x =0.00, and 0.20) nanoparticles.

x	Compound	M_s (emu/g)	M_r (emu/g)	H_c (O_e)
0.00	$Mn_{0.25}Mg_{0.75}Fe_2O_4$	28.98	10.95	61.50
0.20	$Ni_{0.20}Mn_{0.05}Mg_{0.75}Fe_2O_4$	23.40	7.54	94.00

3.3. Gas Sensing Features

Figure 5 shows the sensing characteristics and variation of each nano-ferrite sample before exposure to the nitrogen dioxide (NO_2) gas and when exposed to the gas. As can be seen from the figure, the resistance value of the nano-ferrite discs increased when they were exposed to NO_2 gas (gas ON) and subsequently decreased when the exposure was stopped, the gas was closed (gas OFF). At the concentration of 65 ppm of NO_2, the sensor's sensitivity was examined at various operating temperatures (200 ◦C, 250 ◦C, and 300 ◦C). With an oxidizing gas, the operating temperature changes the material's oxidation state and the conductivity of $Ni_xMn_{0.25-x}Mg_{0.75}Fe_2O_4$ nano-ferrite. Table 5 shows that the samples demonstrated high sensitivity to nitrogen dioxide gas at 250 ◦C while it was around 300 ◦C for sample x=0.00.

As shown in the FE-SEM images, the sensitivity of the doped samples increased because it has high roughness. This is in agreement with the findings of Laith and Al-Saadi [20], and Anuj et al. [37]. Additionally, the figure also demonstrates that the $Ni_{0.20}Mn_{0.05}Mg_{0.75}Fe_2O_4$ ferrite compound has the highest gas response of 707.22% at 250 ◦C. Since the sensitivity process in metal oxides occurs through the adsorption of oxygen ions on the surface, doping of Mn by Ni generally often enhances the sensitivity because a lack of oxygen causes the formation of oxygen voids; (When the oxygen concentration in the $Ni_xMn_{0.25-x}Mg_{0.75}Fe_2O_4$ lattice increases, more oxygen ions (O^{-2} and ^{-}O) are adsorbed on the sensor's surface due of the gaps or voids) [20]. In contrast to the pre-adsorbed oxygen and other test gases, NO_2 gas has a greater electron affinity and is a very reactive and oxidizing gas [40]. After the covalent bond between nitrogen and oxygen is formed, NO_2 has an unpaired electron, and remains as one of the atoms with a single unpaired electron. Since nano-ferrites had a short response time (1.2-11.4) s at 200 ◦C and a short recovery time (1.5-4.4) s at 250 ◦C, it is possible to conclude that the sensor has excellent sensing characteristics. The fast response of the sensor could be a result of the small particle size, which caused the particle boundaries to enlarge. The sensitivity, response, and recovery times are tabulated in Table 5.

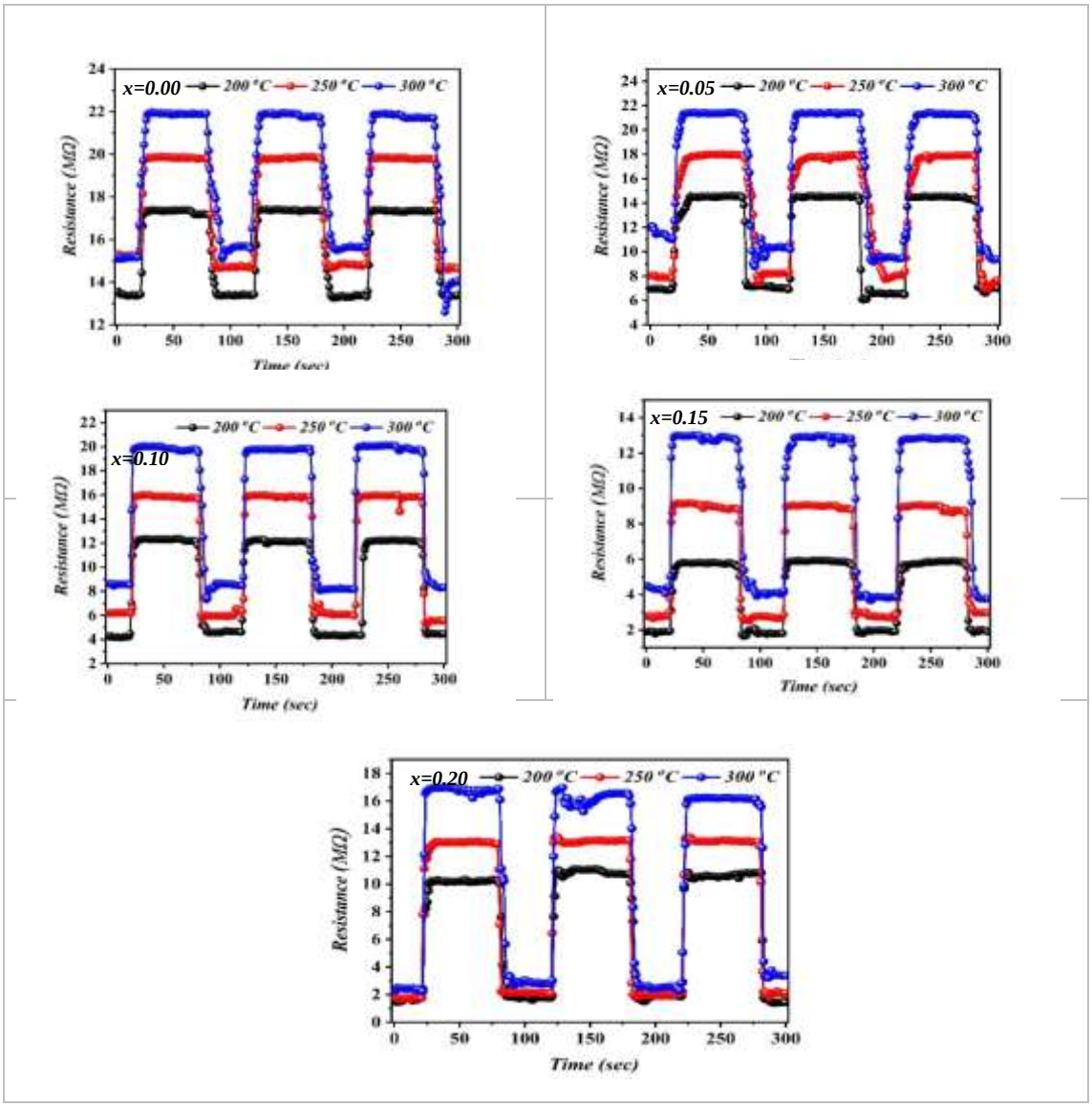

Figure 5: The variation in resistance with time of $Ni_xMn_{0.25-x}Mg_{0.75}Fe_2O_4$ nano-ferrite at different operating temperatures.

Table 5: NO_2 gas sensitivity, response time and recovery time values of $Ni_xMn_{0.25-x}Mg_{0.75}Fe_2O_4$ nano-ferrite at different operating temperatures.

x	Response Time			Recovery Time			Sensitivity %		
	200 ◦C	**250 ◦C**	**300 ◦C**	**200 ◦C**	**250 ◦C**	**300 ◦C**	**200 ◦C**	**250 ◦C**	**300 ◦C**
0.00	2.4	4.0	5.9	5.2	4.4	11.0	30.82	36.30	74.60
0.05	11.4	11.4	5.5	1.9	1.9	6.3	141.72	160.11	134.45
0.10	2.0	1.5	1.9	3.6	1.5	4.7	198.07	202.45	175.34
0.15	11.4	3.2	9.0	9.7	3.0	9.6	262.80	264.28	255.22
0.20	1.2	3.7	1.63	1.8	2.3	5.24	707.34	707.22	676.25

4. Conclusions

$Ni_xMn_{0.25-x}Mg_{0.75}Fe_2O_4$ nano-ferrites were synthesized utilizing a simple sol-gel auto-combustion process using metal nitrates as a source of cations and citric acid ($C_6H_8O_7$) as a complexant/fuel agent for the auto-combustion process. The $Ni_xMn_{0.25-x}Mg_{0.75}Fe_2O_4$ nano-ferrites with the spinel structure had peaks in the XRD patterns corresponding to the investigated systems, and no unidentified peaks were observed. The FE-SEM images showed microstructures with open pores and nanoscale grains with agglomeration, which is nearly comparable to the crystalline size determined by XRD. These findings revealed that, due to the particles being small, the prepared samples at room-temperature hysteresis loop curves exhibited superparamagnetic behavior. Furthermore, the results of the NO_2 gas sensing showed that the gas sensor had a good performance in terms of its response to the gas. The sensitivity increased with increasing the content of Ni in the composition, and showed shorter response and recovery times. For gas sensing applications with $Mn_{0.25}Mg_{0.75}Fe_2O_4$, it was concluded that it is desirable to substitute manganese ions by nickel ions.

References

[1] E. Rossinyol, J. Arbiol, F. Peiro, A. Cornet, J. R. Morante,B Tian, T. Bo, and D. Zhao, "Nanostructured metal oxides synthesized by hard template method for gas sensing applications," *Sens. Actuators B: Chem.*, vol. 109, no. 1, pp. 57-63, 2005

[2] K. Mukherjee and S. B. Majumder, "Reducing gas sensing behavior of nanocrystalline magnesium–zinc ferrite powders," *Talanta*, vol. 81, no. 4-5, pp. 1826-1832, 2010

[3] L. Satyanarayana, K. M.adhusudan Reddy and S. V. Manorama, "Synthesis of nanocrystalline $Ni_{1-x}CoxMn_xFe_{2-x}O_4$: a material for liquefied petroleum gas sensing", *Sens. Actuators B: Chem.*, vol. 89, no. 1-2, pp. 62-67, 2003

[4] A. B. Gadkari, T. J. Shinde, and P. N. Vasambekar, "Effect of Sm^{3+} ion addition on gas sensing properties of $Mg_{1-x}Cd_xFe_2O_4$ system", *Sens. Actuators B: Chem.*, vol. 178, pp. 34-39, 2013

[5] M. Sugimoto, "The past, present, and future of ferrites", *J. Am. Chem. Soc.*, vol. 82, no. 2, pp. 269-280, 2013

[6] D. S. Mathew and Ruey-Shin Juang, "An overview of the structure and magnetism of spinel ferrite nanoparticles and their synthesis in microemulsions", *Chem. Eng. J.*, vol.129, no. 1-3, pp. 51-65, 2007

[7] N. Iftimie, E. Rezlesucu, P. D. Popa and N. Rezlescucu, "Gas sensitivity of nanocrystalline nickel ferrite", *J. Optoelectron. Adv. Mater.*, vol. 8, no. 3, pp. 1016-1018, 2006

[8] Yan-Li Liu, Zhi-Min Lu, Y. Yang, Hai-Feng Yang, Guo-Li Shen and Ru-Qin Yu, "Simple synthesis of $MgFe_2O_4$ nanoparticles as gas sensing materials" *Sens. Actuators B: Chem.*, vol. 107, no. 2, pp. 600-604, 2005

[9] M. Tada, T. Kanemaru, T. Hara, T. Nakagawa, H. Handa, and M. Abe, "Synthesis of hollow ferrite nanospheres for biomedical applications", *J. Magn. Magn. Mater.*, vol. 321, no.10, pp. 1414-1416, 2009

[10] A. Šutka and K. Gross, "Spinel ferrite oxide semiconductor gas sensing", *Sens. Actuators B: Chem.*, vol. 222, pp. 95-105, 2016

[11] Xian-Ming Liu, Shao-Yun Fu and Chuan-Jun Huang, "Magnetic properties of Ni ferrite nanocrystals dispersed in the silica matrix by sol–gel technique", *J. Magn. Magn. Mater.*, vol. 281, no. 2-3, pp. 234-239, 2004

[12] Beyong-Hwan Ryu, Hyun-Ju Chang, Young-Min Choi, Ki-Jeong Kong, Jeong-O Lee, G. K. Chang, Ha-Kyun Jung, and Jong-Hoon Byun, "Preparation of $Co_{1-x}Ni_xFe_2O_4$ nanoparticles by coprecipitation method", *Phys. Status Solidi.(a),* vol. 201, no. 8, pp. 1855-1858, 2004

[13] A. C. F. M. Costa, M. R. Morelli, and R. H. G. AKiminami, "Microstructure and magnetic properties of $Ni_{1-x}Zn_xFe_2O_4$ synthesized by combustion reaction", *J. Mater. Sci.,* vol. 42, no. 3, pp. 779-783, 2007

[14] X. Peng, J. Xu, H. Zang, B. Wang and Z. Wang, "Structural and PL properties of Cu-doped ZnO films", *J. Lumin.*, vol. 128, no. 3, pp. 297-300, 2008

[15] A. B. Bodade, A. B. Bodade, H. G. Wankhade, G. N. Chaudhari and D. C. Kothari, "Conduction mechanism and gas sensing properties of $CoFe_2O_4$ nanocomposite thick films for H_2S gas", *Talanta*, vol. 89, pp. 183-188, 2012

[16] L. Saheb, "Synthesis of (MFe_2O_4) Ferrite as a Gas Sensor", Ph.D thesis, Iraq ,University of Baghdad, College of Education for Pure Science / Ibn Al-Haitham, Department of Physics, 2021

[17] K. Vijaya Kumar, M. Lakshmi and M. Buchi Suresh, "Structure-property correlation of sol–gel processed Co0.5Ti0.5ZnFeO4", Int. j. Eng. Res. Appl., vol. 3, no. 6, pp. 1489-1497, 2013

[18] A. Elahi, M. Ahmad, I. Ali and M. U. Rana, "Preparation and properties of sol–gel synthesized Mg-substituted Ni2Y hexagonal ferrites", Ceram. Int., vol. 39, no. 2, pp. 983-990, 2013

[19] M. Lakshmi, K. Vijaya Kumar and K. Thyagarajan, "An investigation of structural and magnetic properties of Cr–Zn ferrite nanoparticles prepared by a sol–gel process", J. Nanostructure Chem, vol. 5, no. 4, pp. 365-373, 2015

[20] L. Saheb and T. M. Al-Saadi, "Synthesis, Characterization, and NH_3 Sensing Properties of ($Zn_{0.7}Mn_{0.3-x}Ce_xFe_2O_4$) Nano-Ferrite", *J Phys Conf Ser*, vol. 2114, no. 1, p. 012040, 2021

[21] F. Tudorache, E. Rezlescu, P. D. Popa and N. Rezlescu, "Study of some simple ferrites as reducing gas sensors", *J. Optoelectron. Adv. Mater.*, vol. 10, no. 7, pp. 1889-1893, 2008

[22] Lalchand A. Patil, Anil R. Bari, Mahendra D. Shinde, Vinita V. Deo, and Dinesh P. Amalnerkar, "Synthesis of ZnO nanocrystalline powder from ultrasonic atomization technique, characterization, and its application in gas sensing", *IEEE Sens. J.*, vol. 11, no. 4, pp. 939-946, 2011

[23] Myung Sik Choi, Han Gil Na, Jae Hoon Bang, Ali Mirzaei, Seungmin Han, Ha Young Lee, Sang Sub Kim, Hyoun Woo Kim, and Changhyun Jin, "SnO_2 nanowires decorated by insulating amorphous carbon layers for improved room-temperature NO_2 sensing", *Sens. Actuators B: Chem.*, vol. 326, p. 128801, 2021

[24]M. Donarelli, S. Prezioso, F. Perrozzi, F. Bisti, M. Nardone and L. Giancaterini C. Cantalini, L. Ottaviano, "Response to NO_2 and other gases of resistive chemically exfoliated MoS_2- based gas sensors", *Sens. Actuators B: Chem.*, vol. 207, part A,pp. 602-613, 2015

[25]F. Naaz, H. K. Dubey, Ch. Kumari, and P. Lahiri, "Structural and magnetic properties of $MgFe_2O_4$ nano powder synthesized via co-precipitation route", *SN Appl. Sci.*, vol. 2, p. 808, 2020

[26] T. M. Al-Saadi, and A. K. M. Jihad, "Preparation of Graphene Flakes and Studying Its Structural Properties", *Iraqi J. Sci.*, vol. 57, no. 1A, pp. 145-153, 2016

[27]L. Yu, A. Sun, and L. Shao, "Annealing temperature on the microstructure and magnetic properties of magnesium–cobalt ferrite prepared by sol-gel self-propagating method", *J. Mater. Sci.: Mater. Electron.*, vol. 31, pp. 22662-22675, 2020

[28] L. Saheb, and T. M. Al-Saadi, "Study of ($Zn_{0.7}Mn_{0.3-x}Ag_{0.3}Fe_2O_4$) ferrite nanoparticles synthesized by auto combustion method for NO_2 gas sensing", *AIP Conf Proc*, vol. 2591, no. 1, p. 040011, 2023

[29] H. S. Mahmood, T. H. Mubarak, S. M. Ali Ridha, and J. Al-Zanganawee, "Effect of Zinc Substitution in Magnetic Structure on Heat Efficiency for Hyperthermia: Investigation in Superparamagnetic Properties", *AIP Conf Proc*, vol. 2386, p. 070006, 2022

[30] H. J. Mustafa, and T. M. Al-Saadi, "Effects of Gum Arabic-Coated Magnetite Nanoparticles on the Removal of Pb Ions from Aqueous Solutions", *Iraqi J. Sci.*, vol. 62, no. 3, pp. 889-896, 2021

[31] M. Hamedoun, A. Benyoussef and M. Bousmina, "Magnetic properties and phase diagram of $Zn_xNi_{1-x}Fe_2O_4$: high temperature series expansions", *J. Magn. Magn. Mater.*, vol. 322, no. 21, pp. 3227-3235, 2010

[32] A. Sutka, G. Mezinskis, A. Lusis and M. Stingaciu, "Gas sensing properties of Zn-doped p-type nickel ferrite", *Sens. Actuators B: Chem.*, vol. 171-172, pp. 354-360, 2012

[33]I. H. Gul, W. Ahmed and A. Maqsood, "Electrical and magnetic characterization of nanocrystalline Ni–Zn ferrite synthesis by co-precipitation route", *J. Magn. Magn. Mater.*, vol. 320, no. 3-4, pp. 270-275, 2008

[34] S. Raghuvanshi, F. Mazaleyrat and S. N. Kane, "$Mg_{1-x}Zn_xFe_2O_4$ nanoparticles: Interplay between cation distribution and magnetic properties", *AIP Adv.*, vol. 8, no. 4. p. 047804, 2018

[35] M. Abu Haija, A. F.S. Abu-Hani, N. Hamdan, S. Stephen, and A. I. Ayesh, "Characterization of H_2S gas sensor based on $CuFe_2O_4$ nanoparticles", *J. Alloys Compd.*, vol. 690, pp. 461-468, 2017

[36] J. Y. Patil, D. Y. Nadargi, I. S. Mulla and S. S. Suryavanshi, "Cerium doped $MgFe_2O_4$ nanocomposites: highly sensitive and fast response-recoverable acetone gas sensor", *Heliyon*, vol. 5, no. 6, p. e01489, 2019

[37]A. Jain, R. K. Baranwal, A. Bharti**,** Z. Vakil and C. S. Prajapati, "Study of Zn-Cu Ferrite Nanoparticles for LPG Sensing", *Sci. World J.*, vol. 2013, pp. 1-7, 2013

[38] K. Nejati and R. Zabihi, "Preparation and magnetic properties of nano size nickel ferrite particles using hydrothermal method", *Chem. Cent. J.*, vol. 6, no 1, 2012

[39] S. M. Hussein, T. H. Mubarak, S. M. Ali Radha and J. Al-Zanganawee, "Synthesis and Studying Induction Heating of $Mn_{1-x}Zn_xFe_2O_4$ (x = 0 - 0.5) Magnetic Nanoparticles for Hyperthermia Treatments", *Key Eng. Mater.*, vol. 882, pp. 200-218, 2021

[40] N. D. Hoa, N. Van Quy, and D. Kim, "Nanowire structured SnO_x-SWNT composites: high performance sensor for NO_x detection", *Sens. Actuators B: Chem.*, vol. 142, no. 1. pp. 253-259, 2009